



## Plasmonic Bi microspheres doped carbon nitride heterojunction: Intensive photoelectrochemical aptasensor for bisphenol A

Pengcheng Yan <sup>a</sup>, Zhao Mo <sup>a</sup>, Li Xu <sup>a</sup>, Jingyu Pang <sup>b, \*\*</sup>, Junchao Qian <sup>c</sup>, Long Zhao <sup>a</sup>, Jianming Zhang <sup>a</sup>, Jianping Chen <sup>c</sup>, Henan Li <sup>a, \*</sup>

<sup>a</sup> School of the Environment and Safety Engineering, Institute for Energy Research, School of Chemistry and Chemical Engineering, School of Materials Science & Engineering, Key Laboratory of Zhenjiang, Jiangsu University, Zhenjiang, 212013, China

<sup>b</sup> Henan Engineering Research Center of Industrial Circulating Water Treatment, College of Chemistry and Chemical Engineering, Henan University, Kaifeng, 475004, China

<sup>c</sup> Jiangsu Key Laboratory for Environment Functional Materials, Jiangsu Key Laboratory of Intelligent Building Energy Efficiency, Suzhou University of Science and Technology, Suzhou, 215009, China



### ARTICLE INFO

#### Article history:

Received 19 March 2019

Received in revised form

29 May 2019

Accepted 25 June 2019

Available online 26 June 2019

#### Keywords:

Bi microspheres

Carbon nitride

SPR

PEC

Bisphenol A

### ABSTRACT

Considering severe threat of bisphenol A (BPA) to environment and human health, it is urgent to develop a convenient and specific method for accurately detecting BPA. An efficient photoelectrochemical (PEC) aptasensor for determining BPA in water is constructed using Bi microspheres/carbon nitride (Bi/CN) heterojunction as a PEC material. The promoting effect of Bi on the enhanced PEC performance of Bi/CN heterojunction is initiated by two unique effects: the construction of heterojunction (heterojunction effect) and surface plasmon resonance (SPR) effect. For heterojunction effect, a metal-semiconductor heterojunction of Bi/CN is constructed, which increases the light absorption of CN, generates more electron-hole pairs and accelerates the separation of carriers. Simultaneously, as a plasmonic metal, Bi microspheres accelerate charge transfer generated from the heterojunction. This function of Bi is of high benefit to suppress the electron-hole recombination, leading to an enhanced PEC performance. Benefiting from enhanced PEC performance of the heterojunction, a sensitive PEC aptasensor for detecting BPA is realized. This work demonstrates that the Bi/CN heterojunction amplified photoelectric conversion strategy can be used as an efficient method for Bi-based materials to significantly enhance the PEC performance and also provides more opportunities for application of Bi-based materials in PEC field.

© 2019 Elsevier Ltd. All rights reserved.

### 1. Introduction

Photoelectrochemical (PEC) aptasensor has attracted substantial attention through combining photoelectrode with aptamer, due to relatively low cost, miniaturization, fast response, short time and high sensitivity [1]. PEC aptasensor is usually used as an analytical method for monitoring various targets, including small ions, biomolecules and living cells pollutants [2]. The PEC aptasensing process is related to the photoelectric conversion efficiency, depending on the photoinduced carriers separation and transfer of photoactive material [3]. Due to the weak photoelectric conversion efficiency of photoactive materials, the PEC aptasensor is still in its

infancy [4]. Several semiconductors with good optical absorption properties have been used as photoactive materials to construct PEC aptasensor, such as TiO<sub>2</sub> [4], BiOX (X = Cl, Br, I) [3] and ZnO [5], exhibiting good PEC performance. However, most of these materials (TiO<sub>2</sub>, BiOCl and ZnO) only respond to UV light, unable to meet the demand that the PEC aptasensor is often carried out under visible light [4,5]. In order to further widen the application of PEC aptasensor, it is urgent to develop more visible light induced semiconductor materials for constructing PEC aptasensor.

Carbon nitride (CN) holds great promise as an efficient photo-/electrocatalyst for energy conversion, photocatalytic degradation and PEC detection, owing to its appealing electronic structure, high physicochemical stability and earth-abundant compositions [6]. However, its fast recombination of photogenerated electron-hole pairs and unsatisfactory visible light absorption capacity hamper its development in PEC detection field [7]. The construction of heterojunction has proven to be a successful method to increase the

\* Corresponding author.

\*\* Corresponding author.

E-mail addresses: [pjy@henu.edu.cn](mailto:pjy@henu.edu.cn) (J. Pang), [lh@ujs.edu.cn](mailto:lh@ujs.edu.cn) (H. Li).

separation of photogenerated electron-hole pairs [8]. Another effective strategy to enhance the PEC performance of CN is doping noble metals (Au, Ag and Pt) on the surface of CN [9,10]. Several previous reports about Au, Ag and Pt have confirmed that these noble metals are beneficial for improving the PEC performance of semiconductors [8,9]. However, noble metal-based materials used to monitor pollutants are quite expensive and not conducive to industrial-scale applications [11]. Therefore, the development of non-noble metal-based PEC materials becomes a tendency and attracts tremendous interest [8,12,13]. Metallic Bi possesses a series of advantages, including low effective mass, large mean free path, high carrier motility, high earth abundance and low cost, which makes it can be regarded as a promising alternative of Au, Ag and Pt [14]. Metallic Bi has been combined with various semiconductors, such as BiOCl, BiOI and BiVO<sub>4</sub>, showing excellent PEC performance [15,16]. The reason of this phenomenon is often considered as the surface plasmon resonance (SPR) effect of metallic Bi accumulates photogenerated electrons and accelerates the carrier's separation [8,15,16]. In fact, metallic Bi has been confirmed to possess not only SPR effect but also heterojunction effect with some semiconductors [16]. Metallic Bi with heterojunction effect has been discovered to reinforce the visible light adsorption and promote the carrier's separation, resulting in excellent PEC performance [17,18]. Several reports have also confirmed that the visible light induced electrons from Bi nanoparticles transferred to the conduction band (CB) of semiconductor, resulting in effective separation of photoinduced carriers [19,20]. In view of the dual function of Bi, i.e. heterojunction effect and SPR effect, a PEC aptasensor designed by Bi microspheres/CN (Bi/CN) heterojunction for specifically determining bisphenol A (BPA) is expected.

## 2. Experimental section

### 2.1. Material and reagents

All chemicals belonging to analytical grade were used without further purification. Urea, ethylene glycol, absolute ethanol, polyvinylpyrrolidone (PVP), BPA, bismuth nitrate pentahydrate (Bi(NO<sub>3</sub>)<sub>3</sub>·5H<sub>2</sub>O) and nitric acid (HNO<sub>3</sub>) were supplied by Sino-pharm Chemical Reagent Corporation (Shanghai, P. R. China). The BPA aptamer was purchased from Shanghai Sangon Biotechnology Co. Ltd. (Shanghai, China) with the following sequences: 5'-CCG GTG GGT CAG GTG GGA TAG CGT TCC GCG TAT GGC CCA GCG CAT CAC GGG TTC GCA CCA-3'. Distilled water was originated from an ultrapure water system.

### 2.2. Preparation of PEC active materials

CN was prepared via a polycondensation of urea. Urea (3.0 g) was heated at 350 °C for 120 min in a nitrogen atmosphere with a ramping rate of 1 °C min<sup>-1</sup>. Following, it was calcined at a temperature of 600 °C for 240 min using a heating rate of 1 °C min<sup>-1</sup>. The sample was cooled naturally to room temperature, smashed into powders, and set aside.

Bi/CN heterojunction was synthesized by a simple solvothermal method assisted with ethylene glycol as a reducing agent. Bi(NO<sub>3</sub>)<sub>3</sub>·5H<sub>2</sub>O (0.121 g) and HNO<sub>3</sub> (1 mol L<sup>-1</sup>, 3.4 mL) were dissolved into ethylene glycol (16.6 mL) under mechanically stirring for 10 min. Then, PVP (0.2 g) was added into the solution with stirring continuously for another 30 min. CN (0.2 g) was ultrasonically dispersed in the above-mentioned mixture for 30 min. The suspension was transferred into a 25 mL Teflon vessel with 80% volume filling degree. The temperature was increased to 160 °C and kept for 12 h. After naturally cooling down to room temperature,

the sample was collected and washed several times with distilled water and alcohol, respectively. Finally, the cleaned sample was placed into the oven (60 °C) to dry overnight and spare.

### 2.3. Characterization instruments

X-ray diffraction (XRD) spectra were recorded on a Bruker D8 diffractometer using Cu-K $\alpha$  radiation as the source to analyze the crystal phase composition of the samples. Fourier transform infrared (FT-IR) spectra were acquired on the FT-IR spectrometer (Avatar 470, Thermo Nicolet) by the KBr method at wavenumbers 400–4000 cm<sup>-1</sup>. X-ray photoelectron spectroscopy (XPS) measurement was performed on an ESCALab MKII X-ray photo-electron spectrometer. All energy spectra were corrected using the contaminant carbon (C 1s = 284.6 eV) as a reference. Scanning electron microscopy (SEM) images were observed on a JEOL JSM-7001F instrument coupled with an energy dispersive X-ray spectroscope. The UV-vis diffuse reflectance spectroscopy (DRS) spectra of the samples were measured on a UV-2450 spectrophotometer (Shimadzu Corporation, Kyoto, Japan) using a diffuse reflectance method with BaSO<sub>4</sub> powder functioning as the substrate. The photoluminescence (PL) spectra were recorded on a Varian Cary Eclipse spectrometer.

### 2.4. Fabrication of the modified electrodes

Prior to each modification, the indium-tin-oxide conductive glass (ITO) was boiled in a NaOH solution (1 mol L<sup>-1</sup>) for 15 min, rinsed with distilled water and the ethanol solution. Then, it was respectively placed in the distilled water and the ethanol solution for ultrasonically cleaning for 30 min, and naturally dried. The area of cleaned ITO was fixed at 0.5 cm<sup>2</sup> using 3 M tape. The electrode modification process was as follows: The Bi/CN dispersion (50  $\mu$ L, 1 mg mL<sup>-1</sup>) with distilled water as dispersant was coated on the ITO and dried naturally. For contrast, CN/ITO was prepared with the same method. For the preparation of the aptamer/Bi/CN/ITO electrode, Bi/CN/ITO was coated with BPA aptamer (20  $\mu$ L, 1  $\mu$ mol L<sup>-1</sup>), and incubated at normal temperature for 12 h. Then, it was rinsed adequately with distilled water to remove excess BPA aptamer. The fabricated aptamer/Bi/CN/ITO was dried under nitrogen gas and used for further studies. Moreover, the corresponding aptamer/CN/ITO electrode was also prepared using the same method.

### 2.5. PEC measurements

All the PEC experimental results were obtained from a Chenhua instrument CHI660E electrochemical workstation equipped with a 150 W xenon lamp as the visible light source. This PEC device was a constructed three electrode system, where a platinum wire acted as a counter electrode, an Ag/AgCl/sat. KCl functioned as a reference electrode, and the samples modified ITO were used as the working electrode. The electrolyte was a phosphate buffer solution (0.1 mol L<sup>-1</sup>, pH 7.0). The transient photocurrent of the samples was examined for several on-off cycles of the light irradiation. During this testing process, the photocurrent increased sharply with the light irradiation. The photocurrent decreased quickly to its dark current state when the light was turned off. All value of photocurrent was obtained by taking the average after doing three parallel experiments to improve the accuracy of the data. Moreover, the electrochemical impedance spectroscopy (EIS) was also recorded on a CHI660E electrochemical workstation. The used electrolyte was made up of a mixed solution containing KCl solution (0.1 mol L<sup>-1</sup>), phosphate buffer solution (0.1 mol L<sup>-1</sup>, pH 7.0) and Fe(CN)<sub>6</sub><sup>3-</sup>/Fe(CN)<sub>6</sub><sup>4-</sup> (5 mmol L<sup>-1</sup>). EIS experiment was performed at the frequency range from 0.01 Hz to 100 kHz with the bias potential

of 0.24 V and the AC amplitude was 5 mV.

### 3. Results and discussion

#### 3.1. Characterization of the samples

The crystalline structure of CN and Bi/CN heterojunction was examined by XRD characterization (Fig. 1a). The strongest diffraction peak of CN at  $2\theta = 27.4^\circ$  is attributed to the (002) surface of graphite carbon nitride, confirming that CN was successfully obtained by calcination of urea [6]. After loading Bi microspheres on the surface of CN, a series of characteristic peaks are matched with the XRD standard card of metallic Bi (JCPDS No. 44-1246), indicating Bi/CN heterojunction was successfully synthesized through a simple solvothermal method, in which ethylene glycol functioned as a weak reducing agent for the reduction of  $\text{Bi}^{3+}$  to Bi microspheres. In addition, all characteristic peaks of CN are shown in FT-IR spectra of Bi/CN heterojunction (Fig. 1b). The strong peaks at  $1000\text{--}1650\text{ cm}^{-1}$  correspond to the C=N and C–N telescopic vibration of CN [7]. The peak near  $810\text{ cm}^{-1}$  is the flexural vibration peak of three azine ring compounds [10]. These suggest that Bi microspheres introduced to CN did not affect the main structure of CN.

XPS analysis was employed to further investigate the composition and the existing state of elements in Bi/CN heterojunction (Fig. 2). Fig. 2a shows the survey XPS spectra of Bi/CN heterojunction, suggesting that the Bi/CN heterojunction is mainly composed of Bi, C and N elements. A small amount of O element is attributed to the adsorption of water or the absorption of  $\text{CO}_2$  on the surface of Bi/CN heterojunction [3]. The appearance of two peaks at 156.9 and 162.2 eV (Fig. 2b) is assigned to Bi 4f 7/2 and Bi 4f 5/2, indicating that Bi exists in metallic forms as  $\text{Bi}^0$  [3,17]. The peaks in high resolution C 1s spectrum (Fig. 2c) can be divided into two peaks, where the peak at 284.8 eV corresponds to carbon contamination, and the other peak at 288.3 eV belongs to the typical aromatic N–C–N coordination. These two characteristic peaks are the main forms of C existence in the CN based material, implying the successful preparation of CN [21]. Moreover, the peaks of N 1s (Fig. 2d) can be divided into three peaks at the energy of 398.8, 400.4 and 401.5 eV, which represent  $\text{sp}^2$ -hybridized nitrogen (C=N–C), tertiary nitrogen (N–(C)<sub>3</sub>) and terminal amino functions (C–N–H), respectively [3]. The results of XRD, FT-IR and XPS analysis demonstrate that the Bi microspheres were successfully introduced to CN without affecting the main structure of CN.

The micromorphology of CN and Bi/CN heterojunction was carried out by SEM characterization (Fig. 3). Pure CN exhibits

graphite like planar structure with the curled surface (Fig. 3a). Fig. 3b presents the SEM image of Bi/CN heterojunction, in which Bi microspheres are loaded on the surface of CN nanosheets with the size of appropriately 110 nm.

#### 3.2. Optical absorption and photoluminescence properties

The DRS spectra of pure CN, Bi microspheres and Bi/CN heterojunction were tested (Fig. 4a) to evaluate the influence of Bi microspheres on the optical properties of semiconductor materials. Pure CN possesses good absorption in the ultraviolet (UV) light, but weak absorption in the visible light region. The absorption band of the pure CN is 425 nm with the corresponding band gap of 2.8 eV (Fig. S1a), which is consistent with the results in the reported literature [19,22]. Bi microspheres also present an intense absorption both in the UV-light and the visible-light region. It must be noted that, a wide peak at around 500 nm confirms that the plasmonic absorption band of Bi microspheres still falls into the visible light range [17]. After inducing Bi microspheres on the surface of the CN, an obvious increase in the absorbance, occurring in UV and visible light area and contributing to generating electron-hole pairs of Bi/CN heterojunction, resulting into the enhanced PEC performance. The PL spectroscopy of CN and Bi/CN heterojunction were carried out to investigate the recombination efficiency of photo-generated charge carriers (Fig. 4b). Compared to CN, the lower PL emission intensity of Bi/CN heterojunction indicates the lower photogenerated charge carrier recombination efficiency. The PL result indicates that the Bi/CN heterojunction possesses fast separation rate of photogenerated charge carriers, which contributes to the enhancement of PEC performance.

#### 3.3. PEC measurements

The CN and Bi/CN heterojunction were modified onto the ITO electrode, forming CN/ITO and Bi/CN/ITO electrode, respectively. Then, the BPA aptamer was immobilized on Bi/CN/ITO electrode surface, forming aptamer/Bi/CN/ITO electrode. EIS spectra of CN/ITO and Bi/CN/ITO electrode are shown in Fig. 5a, which is used to explore the interface charge transfer of different electrode surface. In the inset of Fig. 5a, the equivalent circuit contains solution resistance ( $R_s$ ), interfacial capacitance ( $C_{dl}$ ), charge transfer resistance ( $R_{ct}$ ) and Warburg impedance ( $Z_w$ ), and the corresponding values of them are listed in Table S1. The semicircular arc diameter of the Bi/CN/ITO ( $R_{ct}$  value of  $262\ \Omega$ ) is smaller than that of CN/ITO ( $R_{ct}$  value of  $1312\ \Omega$ ), indicating low transmission resistance and high charge transfer efficiency of Bi/CN/ITO. This result is attributed

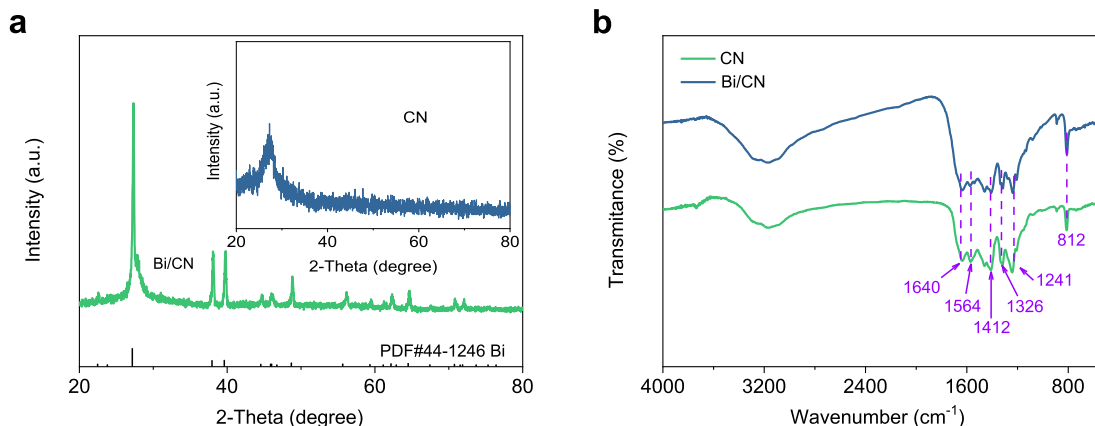


Fig. 1. XRD (a) and FT-IR spectra (b) of the CN and Bi/CN heterojunction.

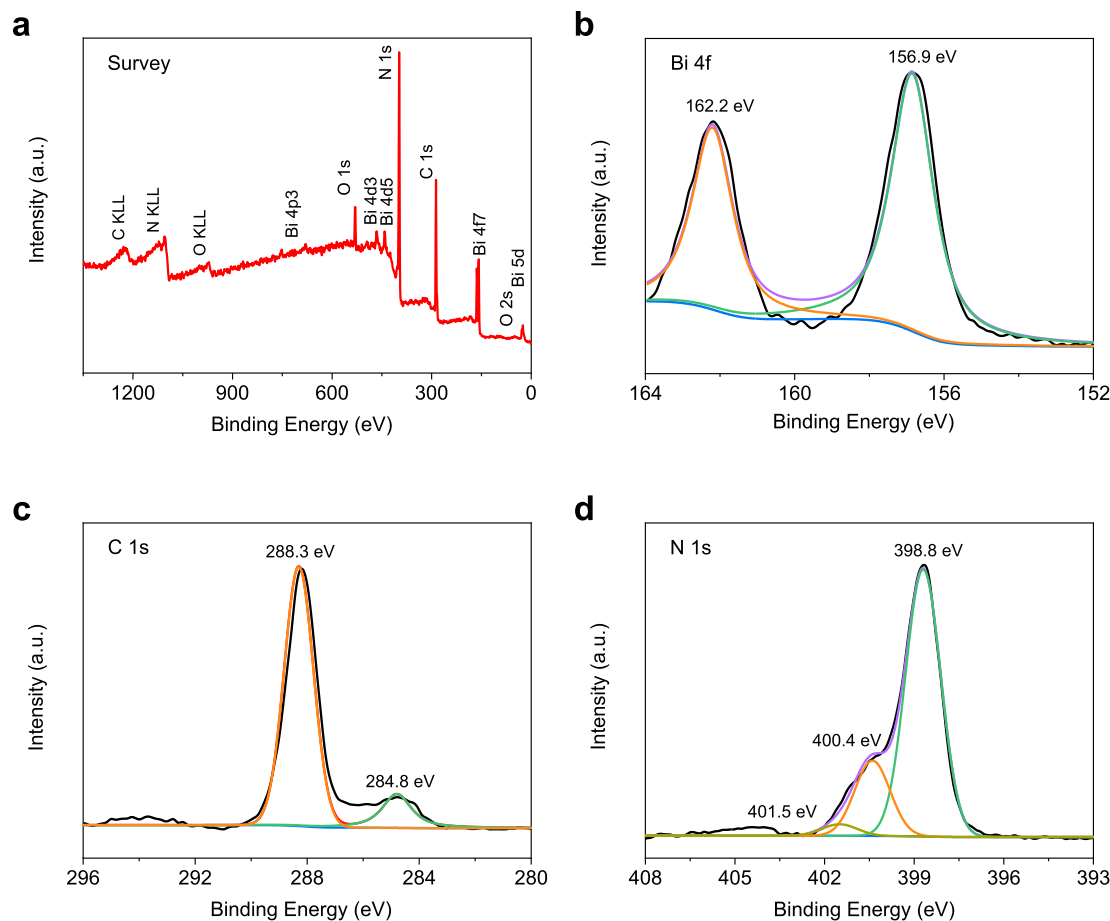


Fig. 2. XPS spectra of Bi/CN heterojunction: (a) survey, (b) Bi 4f, (c) C 1s and (d) N 1s.

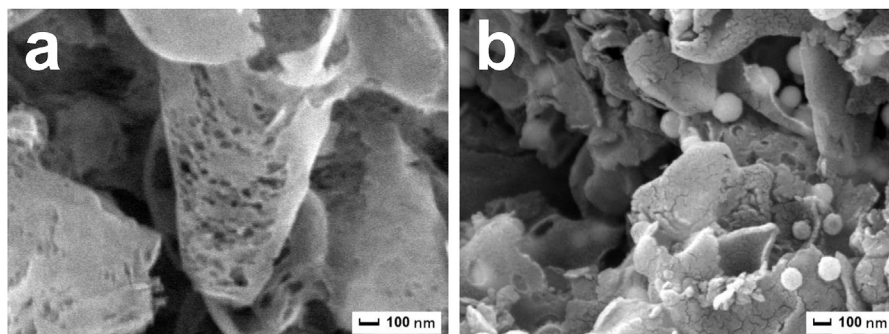


Fig. 3. SEM images of CN (a) and Bi/CN heterojunction (b).

to the introduction of Bi microspheres on the surface of CN, which can also promote the migration rate of charges. For constructing a sensitive PEC aptasensor based on Bi/CN heterojunction, the PEC response of CN/ITO, Bi/CN/ITO, aptamer/Bi/CN/ITO and aptamer/Bi/CN/ITO with  $0.2 \text{ ng L}^{-1}$  BPA was first estimated under light illumination (Fig. 5b). CN/ITO shows a low photocurrent with the value of  $0.03 \mu\text{A}$ , and the reason is as follows. The CN is excited under light irradiation to generate electron-hole pairs. Electrons can be transferred to the CB of CN, while the holes are left on the valence band (VB) of CN, resulting in the production of photocurrent. However, the high recombination rate of photogenerated electron-hole pairs and slow carriers transfer rate of CN lead to low photoelectric conversion efficiency. After the introduction of Bi microspheres on

CN, the photocurrent response of the Bi/CN/ITO increases to  $0.75 \mu\text{A}$ , which is attributed to the fast photogenerated electron-hole pair separation of Bi/CN heterojunction. Based on the determination of VB and CB position of the CN (Fig. S1a-c) and the Fermi level position of metallic Bi, the possible mechanism of Bi/CN heterojunction with enhanced PEC response is proposed (Scheme 1), which can be summarized to the dual function of metallic Bi, i.e. heterojunction effect and SPR effect [16,17,23–27]. To be specific, the CB of CN ( $-1.15 \text{ eV}$ ) is more negative than the Fermi level position of metallic Bi ( $-0.17 \text{ eV}$ ), a metal-semiconductor Bi/CN heterojunction will be constructed as a result. The photogenerated electrons would transfer from CN to the metallic Bi. Metallic Bi functions as an electron sink and transforms a cloud of electrons

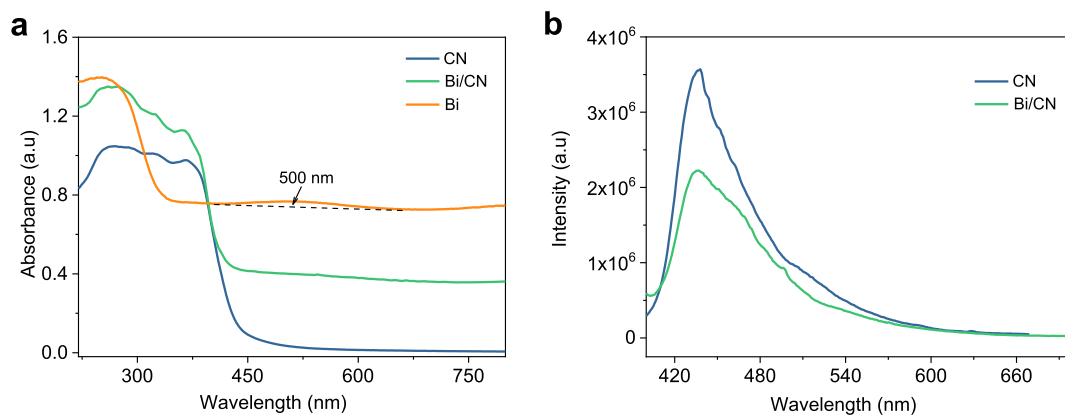


Fig. 4. DRS (a) and PL spectra (b) of the CN and Bi/CN heterojunction.

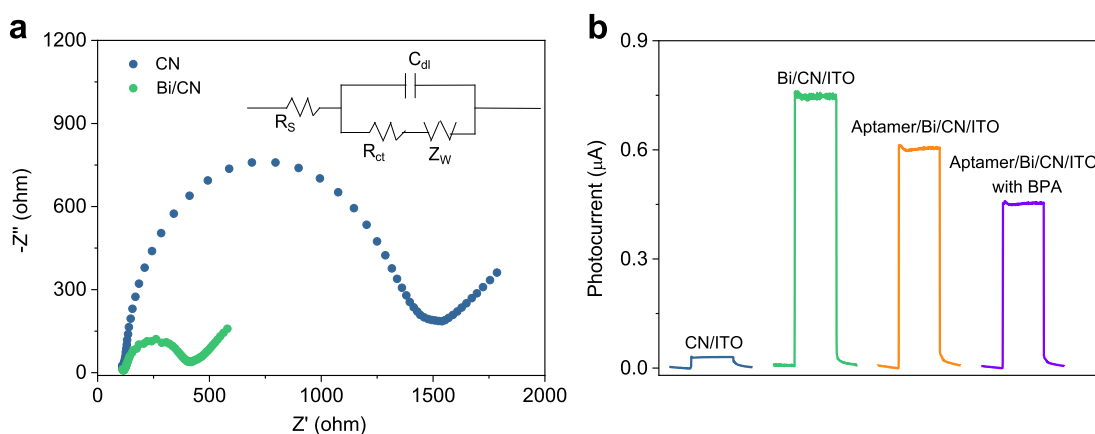
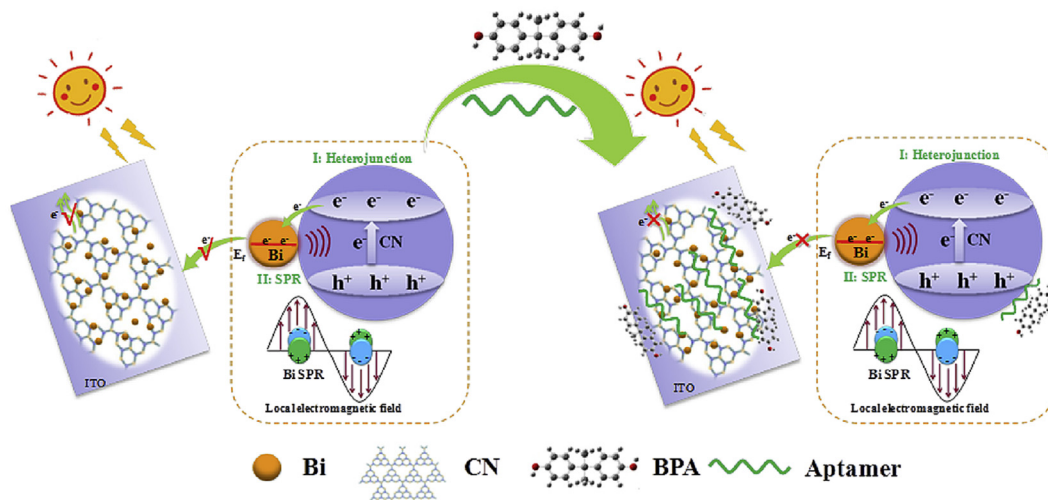


Fig. 5. (a) EIS of CN/ITO and Bi/CN/ITO recorded in a mixed solution containing KCl solution ( $0.1 \text{ mol L}^{-1}$ ), phosphate buffer solution ( $0.1 \text{ mol L}^{-1}$ , pH 7.0) and  $\text{Fe}(\text{CN})_6^{3-}/\text{Fe}(\text{CN})_6^{4-}$  ( $5 \text{ mmol L}^{-1}$ ); (b) Photocurrent response of different electrodes in phosphate buffer solution ( $0.1 \text{ mol L}^{-1}$ , pH 7.0) at  $-0.2 \text{ V}$ .



Scheme 1. The mechanism of the PEC BPA aptasensor based on dual function of Bi, i.e. heterojunction effect and SPR effect at Bi /CN heterojunction.

into ITO electrode to form a circuit. On the other hand, the holes left on the VB of the CN (1.60 eV) migrates to the surface of CN to participate in oxidation reaction. Evidently, the heterojunction effect leads to the efficient separation of photogenerated electron-

hole pairs. Simultaneously, as a plasmonic metal, Bi can generate a local electromagnetic field with the interaction of the semiconductor [26]. That results into an increase in the rates of electron-hole formation on the surface of the CN facilitates electron-hole

pairs separation and enhances the PEC performance. After modifying the BPA aptamer, the photocurrent of aptamer/Bi/CN/ITO is reduced, because that the steric hindrance effect of the BPA aptamer hinders the diffusion of electrons toward the electrode surface [28]. After the aptamer/Bi/CN/ITO was incubated with  $0.2 \text{ ng L}^{-1}$  BPA solution, the photocurrent response was decreased significantly. The decrease of photocurrent is principally because BPA can specifically bind to the aptamer on the Bi/CN/ITO, forming aptamer-BPA complexes cover the surface of the electrode. The steric hindrance of these biomolecules on the electrode interface hinders the electron transfer to the electrode surface and improves the recombination of electron-hole pairs, thereby decreasing the photocurrent. More amounts of BPA will promote more formation of aptamer-BPA complexes, leading to more reduction of photocurrent. The reduced photocurrent can be utilized as a detection signal for quantitative detection of BPA.

Optimizing parameters such as effects of potential and pH of the electrolyte involved in the PEC aptasensor are important to achieve high sensitivity, and optimization experiments were shown in Fig. 6. Fig. 6a shows that the photocurrent of aptamer/Bi/CN/ITO presented a fast-rising tendency at the bias voltage from the range of 0 V to  $-0.3 \text{ V}$ . The photocurrent intensity at  $-0.2 \text{ V}$  is 98% of that at  $-0.3 \text{ V}$ , indicating that the sensitivity of the PEC aptasensor at  $-0.2 \text{ V}$  is sufficient for determining BPA. Considering that low

constant potential is beneficial for the elimination of interference from other species in the samples, an applied potential of  $-0.2 \text{ V}$  is chosen for the subsequent PEC test [29]. In the detection process, the pH of the electrolyte, as one of the important factors affecting the PEC performance, needs to be optimized (Fig. 6b). The photocurrent displays an increasing trend with increasing pH value of the electrolyte from 5 to 7. The photocurrent reduces with the pH value from 7 to 9. It reaches the maximum value at  $\text{pH} = 7$ , probably because that the neutral environment was more conducive to maintaining the activity of the aptamer [30]. Hence,  $\text{pH} = 7$  is selected as the optimum condition for determination of BPA. Under optimum conditions ( $-0.2 \text{ V}$ ,  $\text{pH} = 7$ ), the PEC aptasensor was utilized for determining BPA with different concentration (Fig. 7a). The photocurrent strength decreased with increasing concentration of BPA. In Fig. 7b, there is a good linear relationship between the reduction value of the photocurrent and the logarithmic values of BPA concentration in the range of  $0.02\text{--}2000 \text{ ng L}^{-1}$ . Its linear regression equation was  $I_0 - I = 1.80 \times 10^{-3} \lg C + 3.10 \times 10^{-3}$ . In this equation,  $I_0$  and  $I$  represent the photocurrent value before and after adding BPA, respectively, and  $\lg C$  represents the logarithm of BPA concentration. The detection limit was  $0.0067 \text{ ng L}^{-1}$  ( $S/N = 3$ ). The correlation coefficient ( $R^2$ ) was 0.9932. Comparing with the previously analytic methods of detecting BPA (Table S1), the PEC aptasensor shows a wider linear range and a lower detection limit.

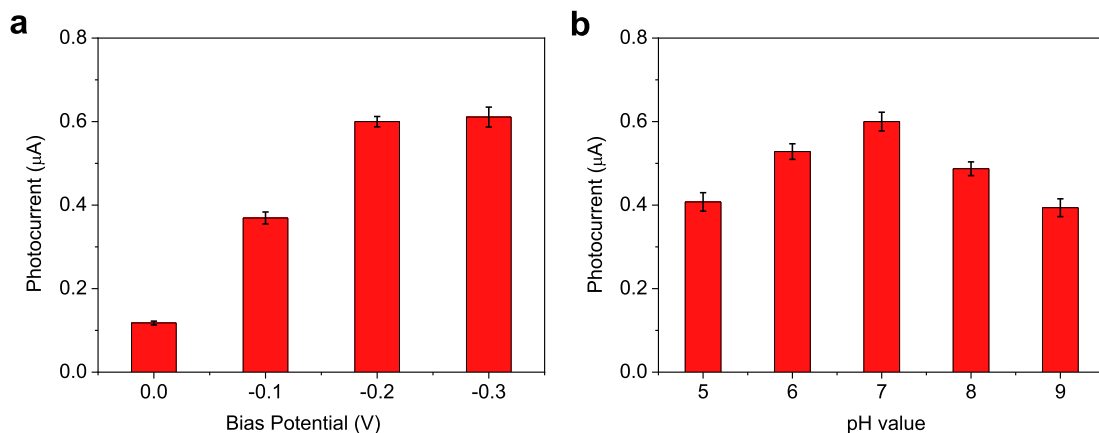


Fig. 6. (a) Effects of potential on photocurrent response of aptamer/Bi/CN/ITO electrode in phosphate buffer solution ( $0.1 \text{ mol L}^{-1}$ ,  $\text{pH} 7.0$ ); (b) Effects of electrolyte pH on photocurrent response of aptamer/Bi/CN/ITO electrode at  $-0.2 \text{ V}$ .

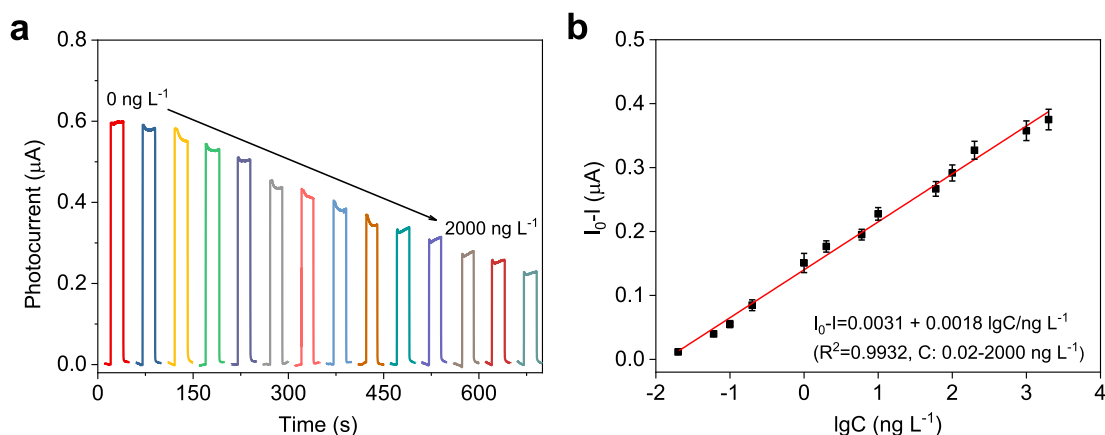
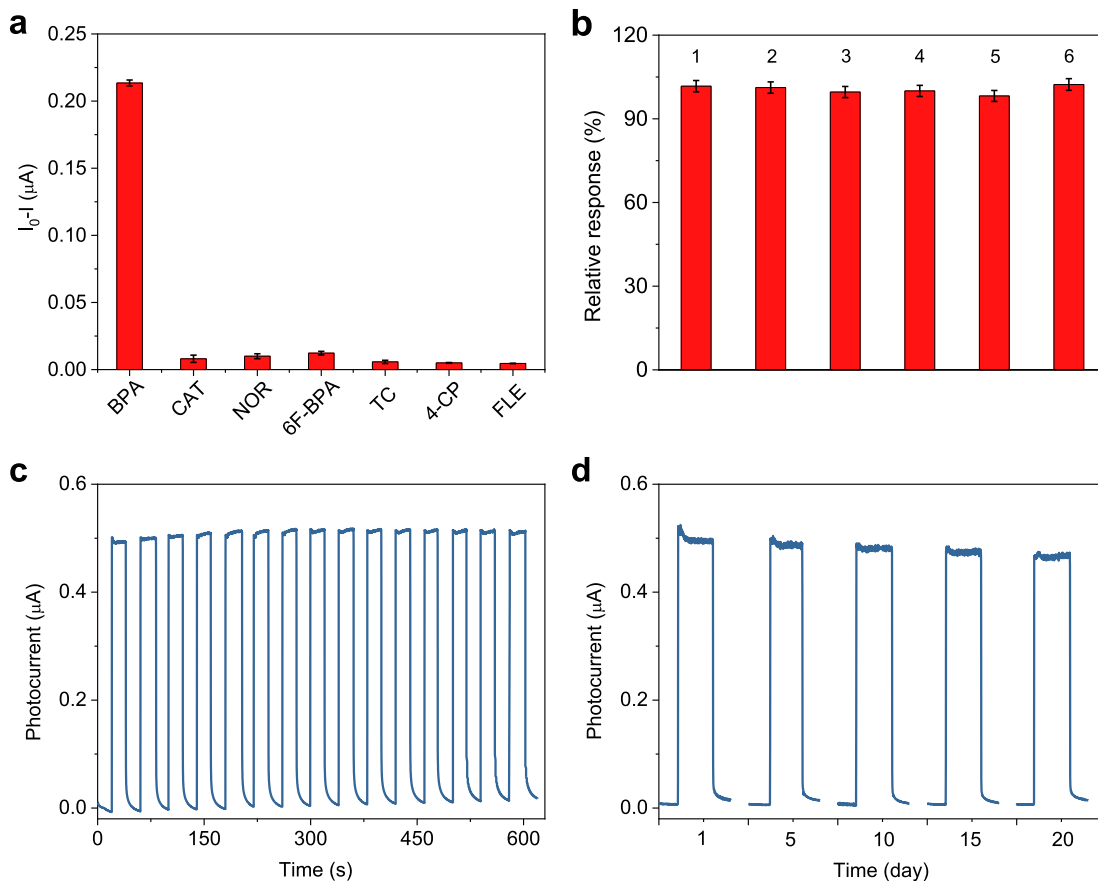


Fig. 7. (a) Photocurrent intensity of the aptamer/Bi/CN/ITO with various concentrations of BPA in phosphate buffer solution ( $0.1 \text{ mol L}^{-1}$ ,  $\text{pH} 7.0$ ) at  $-0.2 \text{ V}$ . BPA concentration: 0, 0.02, 0.06, 0.1, 0.2, 1, 2, 6, 10, 60, 100, 200, 1000, 2000  $\text{ng L}^{-1}$ ; (b) Calibration curve.



**Fig. 8.** (a) The selectivity of the PEC aptasensor among other different interferences; (b) The photocurrent of six individually prepared aptamer/Bi/CN/ITO electrode in the presence of  $0.2 \text{ ng L}^{-1}$  BPA; (c) Time-based photocurrent responses of aptamer/Bi/CN/ITO electrode toward  $0.2 \text{ ng L}^{-1}$  BPA; (d) The change of the photocurrent of aptamer/Bi/CN/ITO electrode in the presence of  $0.2 \text{ ng L}^{-1}$  BPA within 20 days in phosphate buffer solution ( $0.1 \text{ mol L}^{-1}$ , pH 7.0) at  $-0.2 \text{ V}$ .

It suggests that the PEC aptasensor is employed to determine BPA with higher sensitivity and a better practical application prospect.

Several common interferences were used to evaluate the anti-interference ability of the PEC aptasensor. Controllable experiments were carried out by successively testing the photocurrent change of the PEC aptasensor in the presence of  $6 \text{ ng L}^{-1}$  BPA,  $60 \text{ ng L}^{-1}$  catechol (CAT), norfloxacin (NOR), hexafluorobisphenol A (6F-BPA), tetracycline (TC), 4-chlorophenol (4-CP) and feroxacin (FLE), respectively (Fig. 8a). Compared with photocurrent variation brought by BPA, the photocurrent change caused by all other interferences is relatively low and can be ignored. It shows that the PEC aptasensor possessed satisfactory selectivity for BPA detection. The reproducibility of this PEC aptasensor was investigated by evaluating the PEC response of six independent aptamer/Bi/CN/ITO electrodes in the same batches toward  $0.2 \text{ ng L}^{-1}$  BPA (Fig. 8b). The photocurrent response of these six electrodes shows a relative standard deviation (R.S.D) of 0.68%, indicating that the PEC aptasensor possesses a good reproducibility. The stability of the PEC aptasensor was also discussed by means of testing the photocurrent value of aptamer/Bi/CN/ITO toward  $0.2 \text{ ng L}^{-1}$  BPA (Fig. 8c and d). Fig. 8c displays that the photocurrent shows a negligible change within 15 times consecutive dark-light cycle and 20 s for each time interval. Photocurrent strength of the aptamer/Bi/CN/ITO remained at 93.9% of the initial value, after placed in  $4^\circ\text{C}$  dark and humid environment for 20 days (Fig. 8d). These results both prove a satisfying stability of the PEC aptasensor. The as-fabricated PEC aptasensor was employed to determine BPA in different water samples for examining the feasibility. The water samples were

added to a known amount of BPA standard solution to detect the recovery of BPA. Table S2 displays the values of BPA in different samples. The recoveries of the results are ranging from 1.8% to 4.2% in water samples. It indicates that the PEC aptasensor possesses high sensitivity to detect BPA and is suitable for determining the relevant real samples.

#### 4. Conclusion

In summary, a sensitive PEC aptasensor for the determination of BPA was constructed by assembling Bi/CN heterojunction as a PEC active material with a BPA aptamer as a biorecognition element. Bi/CN heterojunction was successfully prepared via a facile solvothermal method assisted with ethylene glycol as a reducing agent. The Bi/CN/ITO shows more enhanced PEC performance than CN/ITO. The greatly enhanced PEC performance upon Bi/CN/ITO is initiated by the dual role of Bi, i.e. heterojunction effect and SPR effect. The heterojunction effect depends on that the Fermi level of Bi matches with the energy level of CN. This effect accelerates separation and transfer of photogenerated carriers. Simultaneously, the SPR effect induced by metallic Bi generates a local electromagnetic field, results into an increase in the rates of electron-hole formation on the surface of the CN and promotes the PEC performances. In general, these two effects are responsible for enhanced PEC performance of Bi/CN heterojunction. Due to steric hindrance of the aptamer-BPA complexes hindering the electron transfer and reducing the photocurrent, BPA can be detected by the proposed PEC aptasensor. The PEC aptasensor displayed a low detection, wide

linear range, acceptable stability and high selectivity. In actual water sample analysis, a satisfactory accuracy of the proposed PEC aptasensor was obtained for detecting BPA. In general, the Bi/CN heterojunction amplified photoelectric conversion strategy can be used as an efficient method for Bi-based materials to significantly enhance the PEC performance as well as provides more opportunities for application of Bi-based materials in PEC aptasensor field.

### Acknowledgements

This work has been financially supported by the National Natural Science Foundation of China (No. 21705058, 21703086), the Provincial Natural Science Foundation of Jiangsu (No. BK20170524), Six Talent Peaks Project of Jiangsu Province (XNY-009), China Postdoctoral Science Foundation (2018T110450), High-tech Research Key laboratory of Zhenjiang (SS2018002), a Project Funded by the Priority Academic Program Development of Jiangsu Higher Education Institutions, and the Research Foundation of Jiangsu University (17JDG007).

### Appendix A. Supplementary data

Supplementary data to this article can be found online at <https://doi.org/10.1016/j.electacta.2019.06.146>.

### References

- [1] F.X. Zhang, P. Zhang, Q. Wu, W.J. Xiong, Q. Kang, D.Z. Shen, Impedance response of photoelectrochemical sensor and size-exclusion filter and catalytic effects in  $\text{Mn}_3(\text{BTC})_2/\text{g-C}_3\text{N}_4/\text{TiO}_2$  nanotubes, *Electrochim. Acta* 247 (2017) 80–88.
- [2] P.C. Yan, D.S. Jiang, H.N. Li, M. Cheng, L. Xu, J.C. Qian, J. Bao, J.X. Xia, H.M. Li, Exploitation of a photoelectrochemical sensing platform for catechol quantitative determination using  $\text{BiPO}_4$  nanocrystals/ $\text{BiOI}$  heterojunction, *Anal. Chim. Acta* 1042 (2018) 11–19.
- [3] L. Xu, D.S. Jiang, Y. Zhao, P.C. Yan, J.T. Dong, J.C. Qian, H.Q. Ao, J.W. Li, C. Yan, H.N. Li, Integrated  $\text{BiPO}_4$  nanocrystal/ $\text{BiOBr}$  heterojunction for sensitive photoelectrochemical sensing of 4-chlorophenol, *Dalton Trans.* 14 (2018) 13353–13359.
- [4] L.P. Wang, Y. Meng, Y. Zhang, C.X. Zhang, Q.J. Xie, S.Z. Yao, Photoelectrochemical aptasensing of thrombin based on multilayered gold nanoparticle/graphene- $\text{TiO}_2$  and enzyme functionalized graphene oxide nanocomposites, *Electrochim. Acta* 249 (2017) 243–252.
- [5] H.L. Hou, H.B. Liu, F.M. Gao, M.H. Shang, L. Wang, L.L. Xu, W.Y. Wong, W.Y. Yang, Packaging  $\text{BiVO}_4$  nanoparticles in  $\text{ZnO}$  microbelts for efficient photoelectrochemical hydrogen production, *Electrochim. Acta* 283 (2018) 497–508.
- [6] Z. Mo, H. Xu, Z.G. Chen, X.J. She, Y.H. Song, J.J. Wu, P.C. Yan, L. Xu, Y.C. Lei, S.Q. Yuan, H.M. Li, Self-assembled synthesis of defect-engineered graphitic carbon nitride nanotubes for efficient conversion of solar energy, *Appl. Catal., B* 225 (2018) 154–161.
- [7] J.P. Jing, Z.Y. Chen, C. Feng, Dramatically enhanced photoelectrochemical properties and transformed p/n type of  $\text{g-C}_3\text{N}_4$  caused by K and I co-doping, *Electrochim. Acta* 297 (2019) 488–496.
- [8] P.C. Yan, D.S. Jiang, H.N. Li, J. Bao, L. Xu, J.C. Qian, C. Chen, J.X. Xia,  $\text{BiPO}_4$  nanocrystal/ $\text{BiOCl}$  nanosheet heterojunction as the basis for a photoelectrochemical 4-chlorophenol sensor, *Sens. Actuators, B* 279 (2019) 466–475.
- [9] M. Volokh, G.M. Peng, J. Barrio, M. Shalom, Carbon nitride materials for water splitting photoelectrochemical cells, *Angew. Chem. Int. Ed.* 58 (2018) 6138–6151.
- [10] L. Xu, S.Y. Ling, H.N. Li, P.C. Yan, J.X. Xia, J.X. Qiu, K. Wang, H.M. Li, S.Q. Yuan, Photoelectrochemical monitoring of 4-chlorophenol by plasmonic Au/graphitic carbon nitride composites, *Sens. Actuators, B* 240 (2017) 308–314.
- [11] D.C. Chen, H.Y. Zhang, Y.G. Li, Y.P. Pang, Z.Y. Yin, H.Q. Sun, L.C. Zhang, S.B. Wang, M. Saunders, E. Barker, G.H. Jia, Spontaneous formation of noble- and heavy-metal-free alloyed semiconductor quantum rods for efficient photocatalysis, *Adv. Mater.* 30 (2018) 1803351.
- [12] P.C. Yan, D.S. Jiang, Y.H. Tian, L. Xu, J.C. Qian, H.N. Li, J.X. Xia, H.M. Li, A sensitive signal-on photoelectrochemical sensor for tetracycline determination using visible-light-driven flower-like CN/ $\text{BiOBr}$  composites, *Biosens. Bioelectron.* 111 (2018) 74–81.
- [13] D.H. Wang, Y.Z. Wang, Y. Chen, W. Liu, H.Q. Wang, P.H. Zhao, Y. Li, J.F. Zhang, Y.G. Dong, S.L. Hu, J.L. Yang, Coal tar pitch derived N-doped porous carbon nanosheets by the in-situ formed  $\text{g-C}_3\text{N}_4$  as a template for supercapacitor electrodes, *Electrochim. Acta* 283 (2018) 132–140.
- [14] Q. Zhang, J.F. Mao, W.K. Pang, T. Zheng, V. Sencadas, Y.Z. Chen, Y.J. Liu, Z.P. Guo, Boosting the potassium storage performance of alloy-based anode materials via electrolyte salt chemistry, *Adv. Energy Mater.* 8 (2018) 1703288.
- [15] Q.Z. Wang, J.J. He, Y.B. Shi, S.L. Zhang, T.J. Niu, H.D. She, Y.P. Bi, Designing non-noble/miconductor Bi/ $\text{BiVO}_4$  photoelectrode for the enhanced photoelectrochemical performance, *Chem. Eng. J.* 326 (2017) 411–418.
- [16] G. Zhou, L. Li, G.H. Li, Semimetal to semiconductor transition and thermoelectric properties of bismuth nanotubes, *J. Appl. Phys.* 109 (2011) 114311–114318.
- [17] G.M. Jiang, X.W. Li, M.N. Lan, T. Shen, X.S. Lv, F. Dong, S. Zhang, Monodisperse bismuth nanoparticles decorated graphitic carbon nitride: enhanced visible-light-response photocatalytic NO removal and reaction pathway, *Appl. Catal., B* 205 (2017) 532–540.
- [18] P.C. Yan, L. Xu, D.S. Jiang, H.N. Li, J.X. Xia, Q. Zhang, M.Q. Hua, H.M. Li, Photoelectrochemical monitoring of ciprofloxacin based on metallic Bi self-doping  $\text{BiOBr}$  nanocomposites, *Electrochim. Acta* 259 (2018) 873–881.
- [19] F. Dong, Q.Y. Li, Y.J. Sun, W.K. Ho, Noble metal-like behavior of plasmonic Bi particles as a cocatalyst deposited on  $(\text{BiO})_2\text{CO}_3$  microspheres for efficient visible light photocatalysis, *ACS Catal.* 4 (2014) 4341–4350.
- [20] Y. Sun, Z. Zhao, F. Dong, W. Zhang, Mechanism of visible light photocatalytic  $\text{NO}_x$  oxidation with plasmonic Bi cocatalyst-enhanced  $(\text{BiO})_2\text{CO}_3$  hierarchical microspheres, *Phys. Chem. Chem. Phys.* 17 (2015) 10383–10390.
- [21] Z. Mo, H. Xu, Z.G. Chen, X.J. She, Y.H. Song, J.B. Lian, X.W. Zhu, P.C. Yan, Y.C. Lei, S.Q. Yuan, H.M. Li, Construction of  $\text{MnO}_2$ /Monolayer  $\text{g-C}_3\text{N}_4$  with Mn vacancies for Z-scheme overall water splitting, *Appl. Catal., B* 241 (2019) 452–460.
- [22] G. Zhao, Y.L. Cheng, Y.Z. Wu, X.J. Xu, X.P. Hao, New 2D carbon nitride organic materials synthesis with huge-application prospects in CN photocatalyst, *Small* 14 (2018) 1704138.
- [23] F. Dong, Z.W. Zhao, Y.J. Sun, Y.X. Zhang, S. Yan, Z.B. Wu, An advanced semimetal-Organic Bi Spheres- $\text{g-C}_3\text{N}_4$  nanohybrid with SPR-enhanced visible-light photocatalytic performance for NO purification, *Environ. Sci. Technol.* 49 (2015) 12432–12440.
- [24] Z. Wang, C.L. Jiang, R. Huang, H. Peng, X.D. Tang, Investigation of optical and photocatalytic properties of Bismuth nanospheres prepared by a facile thermolysis method, *J. Phys. Chem. C* 118 (2014) 1155–1160.
- [25] T. Xiong, X. Dong, H.W. Huang, W.L. Cen, Y.X. Zhang, F. Dong, Single precursor mediated-synthesis of Bi semimetal deposited N-doped  $(\text{BiO})_2\text{CO}_3$  superstructures for highly promoted photocatalysis, *ACS Sustain. Chem. Eng.* 4 (2016) 2969–2979.
- [26] S. Patnaik, D.P. Sahoo, K. Parida, An overview on Ag modified  $\text{g-C}_3\text{N}_4$  based nanostructured materials for energy and environmental applications, *Renew. Sustain. Energy Rev.* 82 (2018) 1297–1312.
- [27] Q. Hao, R.T. Wang, H.J. Lu, C.A. Xie, W.H. Ao, D.M. Chen, C. Ma, W.Q. Yao, Y.F. Zhu, One-pot synthesis of C/ $\text{Bi}_2\text{O}_3$  composite with enhanced photocatalytic activity, *Appl. Catal., B* 219 (2017) 63–72.
- [28] J.Q. Li, L. Guo, N. Lei, Q.Q. Song, Z. Liang, Metallic Bi nanocrystal-modified defective  $\text{BiVO}_4$  photoanodes with exposed (040) facets for photoelectrochemical water splitting, *ChemElectroChem* 4 (2017) 2852–2861.
- [29] J.X. Chen, G.C. Zhao, A novel signal-on photoelectrochemical immunosensor for detection of alpha-fetoprotein by in situ releasing electron donor, *Biosens. Bioelectron.* 98 (2017) 155–160.
- [30] D. Jiang, X.J. Du, Q. Liu, L. Zhou, L.M. Dai, J. Qian, K. Wang, Silver nanoparticles anchored on nitrogen-doped graphene as a novel electrochemical biosensing platform with enhanced sensitivity for aptamer-based pesticide assay, *Analyst* 140 (2015) 6404–6411.